Making corrections to your proof

Please follow these instructions to mark changes or add notes to your proof. Ensure that you have downloaded the most recent version of Acrobat Reader from **https://get.adobe.com** so you have access to the widest range of annotation tools.

The tools you need to use are contained in **Annotations** in the **Comment** toolbar. You can also right-click on the text for several options. The most useful tools have been highlighted here. If you cannot make the desired change with the tools, please insert a sticky note describing the correction.

Please ensure all changes are visible via the 'Comments List' in the annotated PDF so that your corrections are not missed.

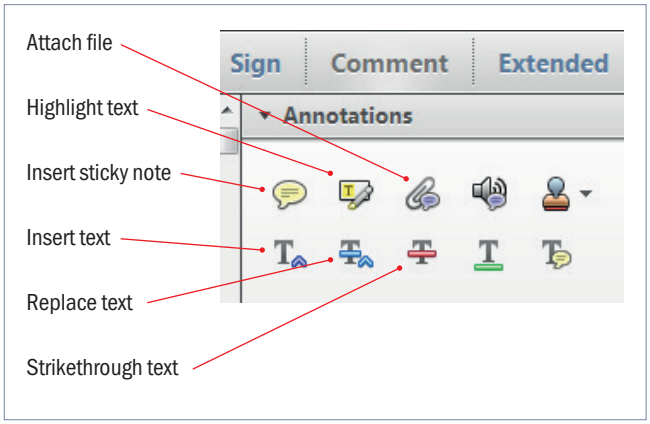

Do not attempt to directly edit the PDF file as changes will not be visible.

Replacing text

To replace text, highlight what you want to change then press the replace text icon, or right-click and press 'Add Note to Replace Text', then insert your text in the pop up box. Highlight the text and right click to style in bold, italic, superscript or subscript.

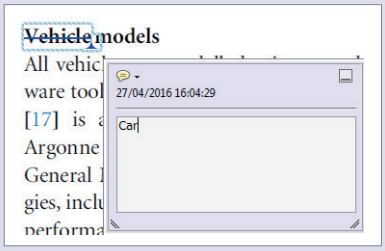

Inserting text

Place your cursor where you want to insert text, then press the insert text icon, or right-click and press 'Insert Text at Cursor', then insert your text in the pop up box. Highlight the text and right click to style in bold, italic, superscript or subscript.

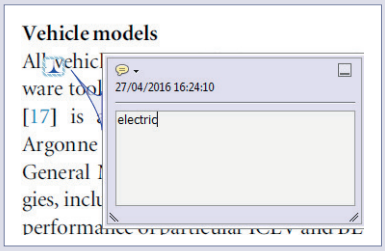

Deleting text

To delete text, highlight what you want to remove then press the strikethrough icon, or right-click and press 'Strikethrough Text'.

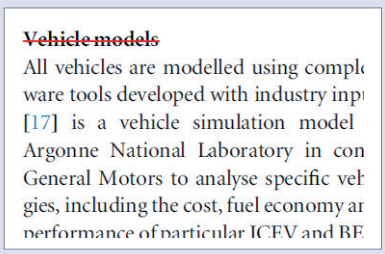

Highlighting text

To highlight text, with the cursor highlight the selected text then press the highlight text icon, or right-click and press 'Highlight text'. If you double click on this highlighted text you can add a comment.

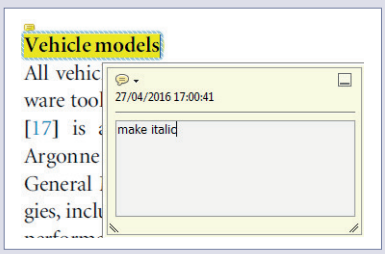

QUERY FORM

JOURNAL: Nanotechnology

AUTHOR: Q D Zhuang *et al*

TITLE: Optically efficient InAsSb nanowires for silicon-based mid-wavelength infrared optoelectronics

ARTICLE ID: nanoaa59c5

The layout of this article has not yet been finalized. Therefore this proof may contain columns that are not fully balanced/ matched or overlapping text in inline equations; these issues will be resolved once the final corrections have been incorporated.

Please check that the names of all authors as displayed in the proof are correct, and that all authors are linked correctly to the appropriate affiliations. Please also confirm that the correct corresponding author has been indicated.

If an explicit acknowledgment of funding is required, please ensure that it is indicated in your article. If you already have an Acknowledgments section, please check that the information there is complete and correct.

SQ1
Please be aware that the colour figures in this article will only appear in colour in the online version. If you require colour in the printed journal and have not previously arranged it, please contact the Production Editor now.

We have been provided with ORCID numbers for the authors as below. Please confirm whether the numbers are correct.
Z M Jin 0000-0001-5523-8153

Please check that the funding information below is correct for inclusion in the article metadata.
Engineering and Physical Sciences Research Council: IAA Lancaster.

Page 5

Q1
Please provide another copy of figure 5 with a correction to the typing error, 'theoretical' instead of 'theoritical'.

Page 6

Q2
Please check the details for any journal references that do not have a link as they may contain some incorrect information. If any journal references do not have a link, please update with correct details and supply a Crossref DOI if available.

Page 6

Q3
Please provide the volume for reference [2].

Page 7

Q4
Please provide the volume and page number or article number in reference [3].

APP Template V1.70 Article id: nanoaa59c5 Typesetter: MPS Date received by MPS: 20/01/2017 PE: MAC004264 CE: LE:

IOP Publishing Nanotechnology

Nanotechnology **00** (2017) 000000 (8pp)

Optically efficient InAsSb nanowires for silicon-based mid-wavelength infrared optoelectronics

Q D Zhuang[1,7], H Alradhi[1], Z M Jin[1], X R Chen[2], J Shao[2,7], X Chen[2], Ana M Sanchez[3], Y C Cao[4], J Y Liu[4], P Yates[5], K Durose[5] and C J Jin[6]

[1] Department of Physics, Lancaster University, Lancaster LA1 4YB, UK
[2] National Laboratory for Infrared Physics, Shanghai Institute of Technical Physics, Chinese Academy of Sciences, 200083 Shanghai, People's Republic of China
[3] Department of Physics, University of Warwick, Coventry, CV4 7AL, UK
[4] Key Laboratory of Optoelectronic Chemical Materials and Devices (Jianghan University), Ministry of Education, Wuhan, 430056, People's Republic of China
[5] Stephenson Institute for Renewable Energy and Department of Physics, University of Liverpool, Liverpool L69 7ZF, UK
[6] State Key Laboratory of Optoelectronic Materials and Technologies, School of Physics and Engineering, Sun Yat-Sen University, Guangzhou 510275, People's Republic of China

E-mail: q.zhuang@lancaster.ac.uk and jshao@mail.stip.ac.cn

Received 22 September 2016, revised 13 January 2017
Accepted for publication 17 January 2017
Published DD MM 2017

Abstract

InAsSb nanowires (NWs) with a high Sb content have potential in the fabrication of advanced silicon-based optoelectronics such as infrared photondetectors/emitters and highly sensitive phototransistors, as well as in the generation of renewable electricity. However, producing optically efficient InAsSb NWs with a high Sb content remains a challenge, and optical emission is limited to 4.0 μm due to the quality of the nanowires. Here, we report, for the first time, the success of high-quality and optically efficient InAsSb NWs enabling silicon-based optoelectronics operating in entirely mid-wavelength infrared. Pure zinc-blende InAsSb NWs were realized with efficient photoluminescence emission. We obtained room-temperature photoluminescence emission in InAs NWs and successfully extended the emission wavelength in InAsSb NWs to 5.1 μm. The realization of this optically efficient InAsSb NW material paves the way to realizing next-generation devices, combining advances in III-V semiconductors and silicon.

Keywords: nanowire, InAsSb, photoluminescence, infrared, molecular beam epitaxy

SQ1 (Some figures may appear in colour only in the online journal)

The monolithic hybrid structure of one-dimensional nanowires (NWs) on silicon has been proposed to be an ideal candidate for advanced silicon-based optoelectronics [1]. Various NW devices have been demonstrated, including solar cells with an efficiency of 14.4% [2], piezoelectric energy generation [3], transistors [4] and lasers [5]. InAsSb NWs have attracted considerable attention in the past few years owing to their potential in the fabrication of silicon-based infrared optoelectronics, in particular, highly efficient room-temperature photodetectors on silicon, which have various important applications, and operate in mid-wavelength infrared (MWIR, i.e. 3–5 μm) and long-wavelength infrared (LWIR, i.e. 8–12 μm). InAsSb alloys possess unique properties such as their direct and widely tunable narrow bandgap energy, high thermal conductivity, small electron effective mass, long carrier lifetime [6], and high electron mobility [7]. On the other hand, their unique 1D architecture has a number of advantages in device applications such as enhanced light

[7] Author to whom any correspondence should be addressed.

absorption [8], long carrier diffusion length [9], improved carrier collection efficiency [10], great degree of freedom in combining materials with different lattice parameters and the doping profiles [11, 12]. These features make InAsSb NWs an ideal and versatile candidate for a variety of device applications, for instance, in optoelectronics in the infrared and terahertz spectral ranges, high-speed electronics, thermophotovoltaic and thermoelectric devices, and cost-effective biosensors.

However, producing high-quality InAsSb NWs with a high Sb content remains a challenge due to the difficulty in incorporating the Sb, and they have poor optical properties caused by the poor crystalline quality of the NWs [13]. Although InAsSb NWs with a whole range of Sb content (0%–100%) have been reported, the photoluminescence (PL) emission wavelength is limited to a wavelength of 4.0 μm at an Sb content of 15% [14]. This is mainly due to the highly dense crystalline defects in the resulting NWs. Different epitaxial techniques have been adopted for high-quality InAsSb NW growth including molecular beam epitaxy (MBE), metal organic chemical vapour deposition (MOCVD) and chemical beam epitaxy (CBE) as well as catalyst-assisted and area selective epitaxy: (i) using MBE, InAsSb NWs were obtained with an Sb content of up to 10% by Zhuang *et al* on silicon [13, 15] and graphite [16], up to 15% by Sourribes *et al* [17] and 35% grown on GaAs (111) by Potts *et al* [18]; (ii) using the MOCVD growth technique, catalyst-free InAsSb NWs with an Sb content of up to 43% have also been reported [19], while selective-area epitaxy on patterned InAs substrates recently demonstrated InAsSb NWs with an Sb content of 15% [14]; (iii) using MOCVD with Au-catalysis, InAsSb NWs with an Sb content of up to 77% have been obtained [20, 21]; and (iv), using Au-catalyzed CBE, InAsSb NWs with a whole range of Sb have been realized [22]. Although there has been significant progress in increasing Sb incorporation, there has been no success in extending the emission wavelength above 4.0 μm. In theory, with the increase of Sb content, the emission wavelength should be extended even further to 12 μm. It should be noted that high Sb content NWs, normally obtained by using catalysts [23–26], have been demonstrated on a number of devices—though NWs grown using both Au-catalysts [27, 28] and Ni-catalysts [29] exhibit degradation in electrical and optical properties. A recent report of 4.0 μm PL emission from MOCVD selective-area-grown InAsSb nanowires [14] shows that there is promising potential for catalyst-free growth to obtain optically active NWs.

Here, we report the realization of optically efficient InAsSb NWs on silicon via advanced droplet-assisted epitaxy. Through optimizing the V/III flux ratio and Sb flux we successfully suppressed the Sb surfactant effect and obtained InAsSb NWs with an Sb content of up to 19%, as well as successfully extending the emission wavelength to 5.1 μm. To the best of our knowledge, we have reported the longest emission wavelength of InAsSb NWs so far: 27.5% longer than the previously reported longest emission wavelength (i.e. 4.0 μm). This achievement enables InAsSb NWs to cover the entire MWIR band. This study opens up a route to utilizing InAsSb NWs in the fabrication of highly sensitive silicon-based room-temperature infrared photodetectors operating in MWIR and LWIR.

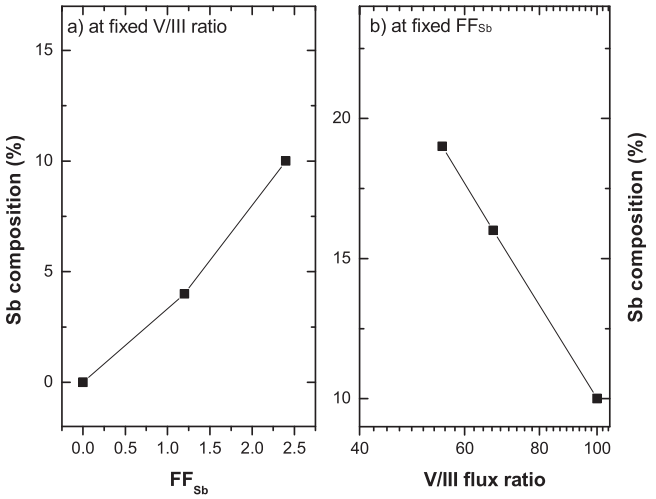

Figure 1. The Sb composition as a function of FF_{Sb} under a V/III flux ratio of 100 (a) and a V/III flux ratio under a FF_{Sb} of 2.4% (b).

The InAsSb NWs were grown by a previously established droplet-assisted growth technique [13, 15]. In this growth technique, the NW growth is initiated from the deposition of indium (In) droplets at pre-optimized conditions acting as the seeding site to prompt the growth of the NWs. It is well known that the epitaxial growth of NWs containing Sb is notoriously difficult due to its strong surfactant effect, so we start with an investigation of Sb incorporation. A series of samples were grown on Si (111) at pre-optimized growth conditions. The Sb composition was mainly controlled by tuning the Sb fractional flux (FF_{Sb}) defined as: $FF_{Sb} + F_{Sb2}/(F_{Sb2} + F_{As4})$, where F_{Sb2} and F_{As4} are the flux of the Sb and As respectively. This was combined with a variation of the V/III flux ratio to achieve higher Sb incorporation.

The geometry of the resulting InAsSb NWs was investigated by scanning electron microscopy (SEM). We have previously obtained $InAs_{0.90}Sb_{0.10}$ NWs at a V/III flux ratio of 100 [13]. Sb incorporation increases linearly with an increasing FF_{Sb}, as shown in figure 1(a). However, a higher FF_{Sb} (4.5%) results in a thin film (see figure 2(b) as the SEM image tilted by 45°). This indicates that an FF_{Sb} which is larger than 2.4% will not result in any NWs under our growth conditions. This observation is consistent with a previous report [17] and is associated with the surfactant effect of Sb, which modifies the kinetics and thermodynamic processes during growth [15]. In order to overcome this effect, we attempted to increase Sb incorporation by tuning other growth parameters, e.g. reducing the V/III flux ratio. Figure 2 shows the SEM images tilted by 45° of the samples grown at a V/III flux ratio of 100 under an FF_{Sb} of 2.4% (a) and 4.6% (b), and at an FF_{Sb} of 2.4% under a V/III ratio of 67 (c) and 55 (d). This shows that growth condition (a) produced $InAs_{0.90}Sb_{0.10}$ NWs, while condition (b) with a higher FF_{Sb} at a V/III ratio of 100 led to thin film. It also shows that a reduced V/III flux ratio favours the growth of NWs and enhances Sb

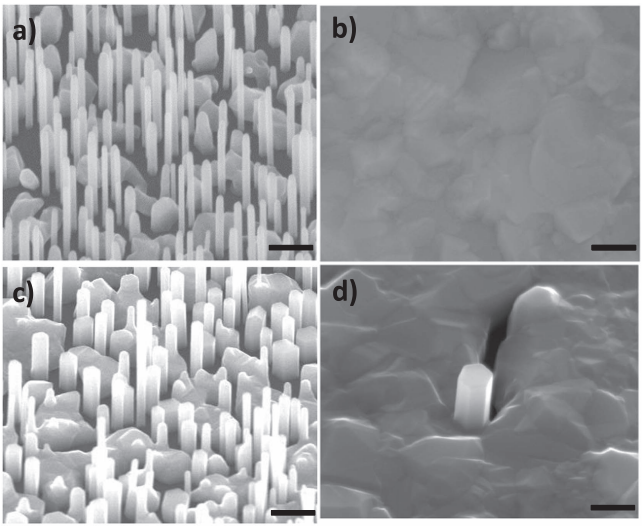

Figure 2. SEM images tilted 45° of InAsSb NWs grown under a V/III ratio of 100 at an FF_{Sb} of 2.4% (a) and 4.5% (b), and at an FF_{Sb} of 2.4% under a V/III ratio of 67 (c) and 55 (d).

incorporation (see figure 3 for the TEM/EDX-determined Sb composition). As shown in figure 1(b), decreasing the V/III flux ratio from 100 to 67 and 55 results in an Sb content of 10%, 16% and 19% respectively. It should be noted that the reduction of the V/III flux ratio was obtained by increasing the growth rate. We believe that a faster growth rate reduces the Sb surfactant effect. Meanwhile, the higher growth rate favours Sb incorporation, which is the same as that observed in the epitaxy of InAsSb thin film [30]. It is worth mentioning that the growth of NWs is sensitive to the V/III flux ratio and growth rate, so special care must be taken with the fine-tuning of the above two factors to maintain a regime of NW growth. Also, Sb incorporation led to short, thick NWs, and a dramatic drop of areal density, while the Sb content is higher than 16%, with drops from $\sim 5 \times 10^9\,\mathrm{cm}^{-2}$ at 16% Sb to $\sim 3 \times 10^7\,\mathrm{cm}^{-2}$ at 19% Sb, which is consistent with a previous report [20]. We correlate this behaviour with the droplet-assisted growth technique used for growth. The preformed droplets act as nucleation sites to proceed to NWs, consequently determining the distribution of the corresponding NWs. This indicates that the droplet-assisted growth technique is promising for obtaining InAsSb nanowires with high areal density.

The Sb composition of the NWs was determined using energy-dispersive x-ray spectroscopy (EDX) measurements in a transmission electron microscope (TEM). High-resolution transmission electron microscope (HRTEM) images were taken in a JEOL-JEM 2100 microscope working at 200 kV. To prepare the specimen for TEM studies, the NWs were scraped from the substrate mechanically and then deposited on a holey carbon grid. Focused ion beam (FIB) specimens were prepared using a JIB4500 for HRTEM measurements. Energy-dispersive x-ray spectroscopy (EDX) measurements were also carried out with an Oxford Instrument X-MAX 80 to determine the elemental composition and fluctuation. For the reliable determination of Sb composition, EDX point analysis was performed on each sample at different positions along a single NW. Four samples with different Sb composition were measured. Figure 3 shows the typical TEM/EDX analysis data of single InAsSb NWs for each of the four samples, with the Sb content for three different positions being shown in the inset table. The NWs have an average Sb content of 3%, 11%, 16% and 19%, but there is also some fluctuation of the Sb content along the length of the NW. Consequently, we performed EDX measurements at many points along the length of each single NW to estimate the composition fluctuation. This data is summarized in table 1 with the relevant PL data and theoretical bandgap energies. These EDX measurements prove the realization of InAsSb NWs with an Sb content of up to 19%. It is worth noting that Sb fluctuation gets larger with the increase of Sb incorporation. The cause of this fluctuation is not clear, but it is most likely related to the modification of Sb incorporation by the kinetics and thermodynamics effects during NW growth. It should be noted that the length of the NW taken by the EDX measurement is much longer than the length determined by the SEM measurements. We believe this is related to the technique we used to catch the NWs for TEM measurements. A copper grid was used to gently scribe the surface of the samples, which results in a much higher chance of catching the longest NWs.

To explore the optical properties of the resulting NWs, we performed PL measurements on a series of as-grown samples with an Sb content of up to 19%. A diode laser emitting at 980 nm was used for excitation. The signal was collected and dispersed by a monochromator and detected by a cooled HgCdTe photodetector through a lock-in amplifier. The power density of the excitation is around $20\,\mathrm{W\,cm}^{-2}$ (a laser power of 200 mW with a laser spot of around 1 mm^2). In addition, an infrared modulated PL method based on a step-scan Fourier transform infrared spectrometer (FTIR) was also used for detailed PL measurements such as temperature-dependent and excitation-dependent scans [31, 32]. Figure 4 depicts the evolution of the low-temperature (10 K) PL spectrum of InAsSb NWs with an increasing Sb composition. Based on the density of the NWs, we estimate that our PL measurement came from a contribution of around 10^6 NWs with a laser spot of 1 mm^2. Strong PL emission was observed for all the samples, and a long wavelength emission of up to 5.1 μm was achieved. It should be noted that the detected PL emission of the samples is believed to originate from the NWs, although there were InAsSb clusters present on the Si surface. To verify that the emission was from the NWs, we removed them using an ultrasonic bath, and as a result no PL emission was detected from the samples. The failure in luminescence of the clusters is associated with their poor material quality, resulting from both the large lattice mismatch and antiphase domains. Several features can be seen in the NW spectra: firstly, with the increase of Sb composition, the spectra progress from multi-peak emission in the InAs NW sample to single peak emission (at an Sb content $\geqslant$10%); secondly, the dominant peak of the samples shifts to lower energy with an increasing Sb content; and thirdly, the full width of half maximum (FWHM) of the PL spectra tends to be broader for the samples with a higher amount of Sb

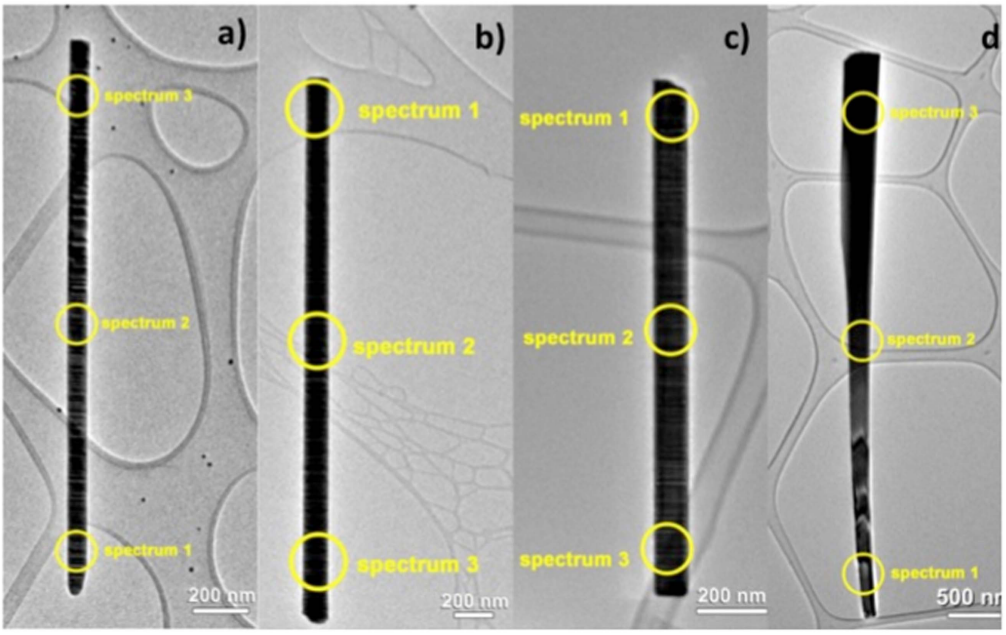

$InAs_{1-x}Sb_x$

Spectrum	1-x (%)	x(%)
1	98	2
2	97	3
3	98	2

$InAs_{1-x}Sb_x$

Spectrum	1-x (%)	x(%)
1	91	11
5	89	11
6	90	12

$InAs_{1-x}Sb_x$

Spectrum	1-x (%)	x(%)
1	83	17
2	84	16
3	85	15

$InAs_{1-x}Sb_x$

Spectrum	1-x (%)	x(%)
1	81	19
2	82	18
3	83	17

Figure 3. An EDX point analysis of a single NW for four samples giving an average Sb content of 3% (a), 11% (b), 16% (c) and 19% (d), with the content at different positions along the NW.

Table 1. The EDX-determined Sb content and the corresponding theoretical bandgap energy for a series of InAsSb NWs with the photoluminescence band-to-band (BtB) related emission peak energy (measured at 10 K) and the FWHM.

	Photoluminescence[a]			Theoretical E_g
Measured Sb content and variation (atm.%)	Peak energy (eV)	FWHM (meV)	Ref	(eV)
0	0.427	30.0	This work	0.417
2 ± 1	0.406	45.5	Ref [31]	0.400 ± 0.014
3 ± 1	0.405	47.4	This work	0.394 ± 0.008
4 ± 1	0.375	48.8	Ref [13]	0.384 ± 0.009
11 ± 2	0.345	66.6	Ref [13]	0.339 ± 0.011
16 ± 3	0.304	66.8	This work	0.297 ± 0.017
19 ± 4	0.242	71.8	This work	0.279 ± 0.022

[a] Estimate uncertainty of 1.0 meV and 1.4 meV for peak energy and FWHM.

incorporation. It is important to note that a long wavelength emission of up to 5.1 μm (an equivalent energy of ~0.242 eV) was obtained for the sample with an Sb composition of 19%. To the best of our knowledge, this is the longest PL emission reported to date for InAsSb NWs.

In figure 4 we also show the decomposition of the PL emission for each sample. One can see that for the samples with an Sb content of 10% and above, only a single peak is visible. The origin of these emissions can easily be assigned to the band-to-band (BtB) transition. However, the samples with a lower Sb content demonstrate multi-peak emission (i.e. the InAs and $InAs_{0.97}Sb_{0.03}$ NWs). Due to the mixture of the crystalline phases in InAsSb NWs, different transition mechanisms co-exist, e.g. impurity- or defect-related transitions [23, 24, 33, 34], type-II transitions due to the WZ/ZB mixture [35, 36] and the BtB transition from ZB InAs. We have already identified the co-existence of all these origins in the InAs NWs [13], and can hence assign the high-energy emission and low-energy emissions originating from the BtB transition and type-II transition respectively. It is worth noting that the defect/impurity-related emission is absent in all the samples. This implies the improved material quality in comparison with the previous samples through further growth optimization. This is correlated to the observation of room temperature PL emission from the InAs NWs. With these assigned origins of the emission peaks, we now focus on the BtB emission peak energy E_p, which reflects the bandgap energy E_g of the InAsSb NWs, which follows a general relation $E_g = E_p - \frac{1}{2}k_B T$, where k_B is the Boltzmann constant. It should be noted that the peak energy of sample E is lower than the apparent peak centred at 0.321 eV because of the strong absorption of CO_2 at 0.282–0.296 eV. With consideration of this absorption, the emission peak energy of $InAs_{0.84}Sb_{0.16}$ is estimated to be 0.304 eV. The BtB-related PL emission peak energy and the lineshape for the samples with different Sb compositions (deduced from EDX) are summarized in table 1. The bandgap energy of the InAsSb alloy as a function of Sb composition is expressed as [37]

$$E_g = xE_{InSb} + (1 - x)E_{InAs} - Cx(1 - x),$$

where x is the Sb composition, E_{InAs} and E_{InSb} are the

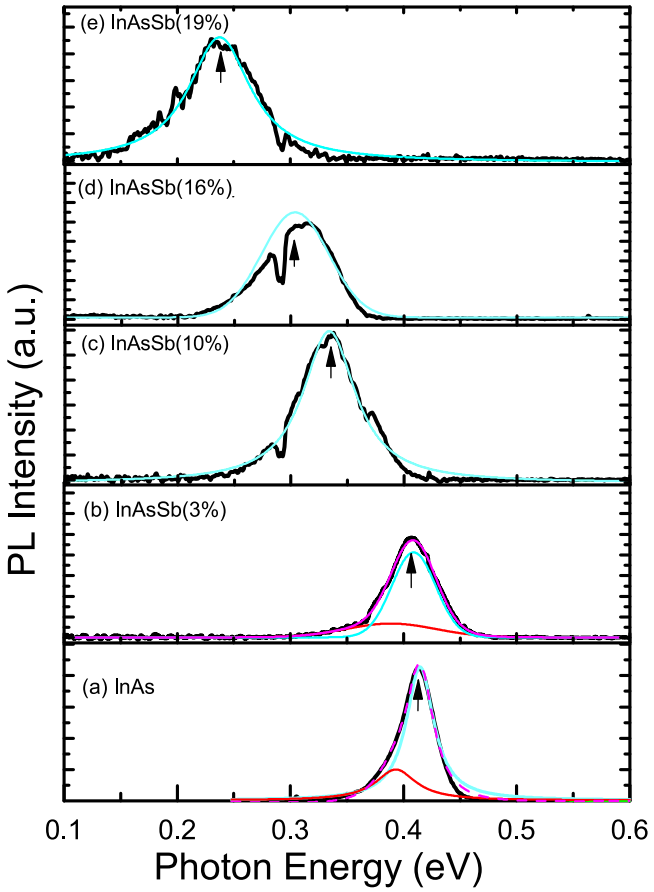

Figure 4. The evolution of 10 K PL of InAs NWs (a) and InAsSb NWs with an Sb composition of 3% (b), 10% (c), 16% (d) and 19% (e). The peaks in colours show the decomposed emissions.

bandgaps at a temperature of 10 K for InAs and InSb respectively, and C is the bowing parameter. It can be seen that the BtB-related emission shows a strong red-shift with an increase in Sb composition, which is attributed to the bandgap shrinkage with the presence of Sb. This bandgap shrinkage is in agreement with the equation above using a bowing parameter of ∼0.67 eV [38], which is between the accepted values of 0.66 eV [14] and 0.682 eV [39]. However, for the InAsSb NWs with a high Sb composition of 19%, the PL-deduced bandgap energy is slightly lower than expected. We correlate this difference with the wider Sb fluctuation in the NWs with higher Sb incorporation, as shown in table 1. Such an Sb fluctuation within the segments could construct a slight type-II alignment, which in turn results in a transition energy that is lower than the bandgap energy of the corresponding bulk materials.

In order to evaluate the optical properties at a high Sb content, we also performed temperature-dependent PL for the sample $InAs_{0.84}Sb_{0.16}$ NWs. Figure 5 shows the PL spectra measured at the evaluated temperature. Emission is visible up to 120 K. A clear red-shift is visible with increasing temperature. The peak energies E_p at different temperatures are depicted in the inset with the corrected energy using $k_BT/2$

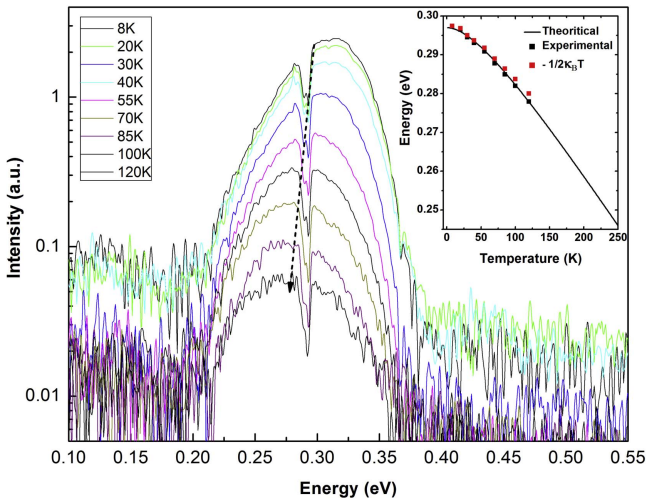

Figure 5. The photoluminescence of $InAs_{0.84}Sb_{0.16}$ NWs measured at various temperatures. The inset is the peak energy E_p, the energy of $E_g - k_BT/2$ and the theoretical bandgap energy.

and the theoretical bandgap energy defined as

$$E_g(T) = E_{g0} - \frac{\alpha T^2}{\beta + T},$$

where $E_g(T)$ is the bandgap energy at 0 K, and α and β are empirically determined parameters which can be considered to have linear functions of x. Using 0.297 eV as E_{g0} for $InAs_{0.84}Sb_{0.16}$, and the experimentally determined values of α and β for InAs and InSb [40], we found that the theoretical bandgap of $InAs_{0.84}Sb_{0.16}$ follows $E_g(T) = E_p - k_BT/2$. It should be noted that the detection of emission is not possible at higher temperatures due to the weak signal. Q1

The efficient optical properties of our NWs—in particular the pure crystal phase and reduced stacking faults—are attributed to the improved crystalline quality of the NWs obtained by the novel technique of droplet-assisted growth. High-resolution TEM (HRTEM) measurements were performed to investigate their crystalline quality. Figure 6 shows the typical HRTEM images of a series of InAsSb NWs with a different Sb content. One can see that all the NWs with an Sb content below 16% show a mixture of the ZB and WZ segments. The average segment size of each phase in each sample was statistically analyzed, revealing a strong dependence on Sb incorporation, as shown in figure 6(e). The prevalent size increases for both ZB and WZ segments with increasing Sb incorporation. For the InAs NWs, the size of the ZB and WZ segments is roughly equal. For the InAsSb NWs with a small amount of Sb, the WZ segment size is slightly larger than that of the ZB, while for the samples with a higher Sb content (16%), the size of the ZB segments is much larger than those of the WZ. More importantly, the sample of NWs with 19% Sb shows a pure-ZB crystal phase. This observation is further confirmed by the corresponding fast Fourier electron diffraction pattern, as depicted in figure 6 (bottom panel). The 111_{ZB} and/or 0002_{WZ} spot indicates the growth direction both in the ZB and WZ phases. The streaks passing through the spots along the growth direction indicate the presence of stacking faults in the structure, lying on the

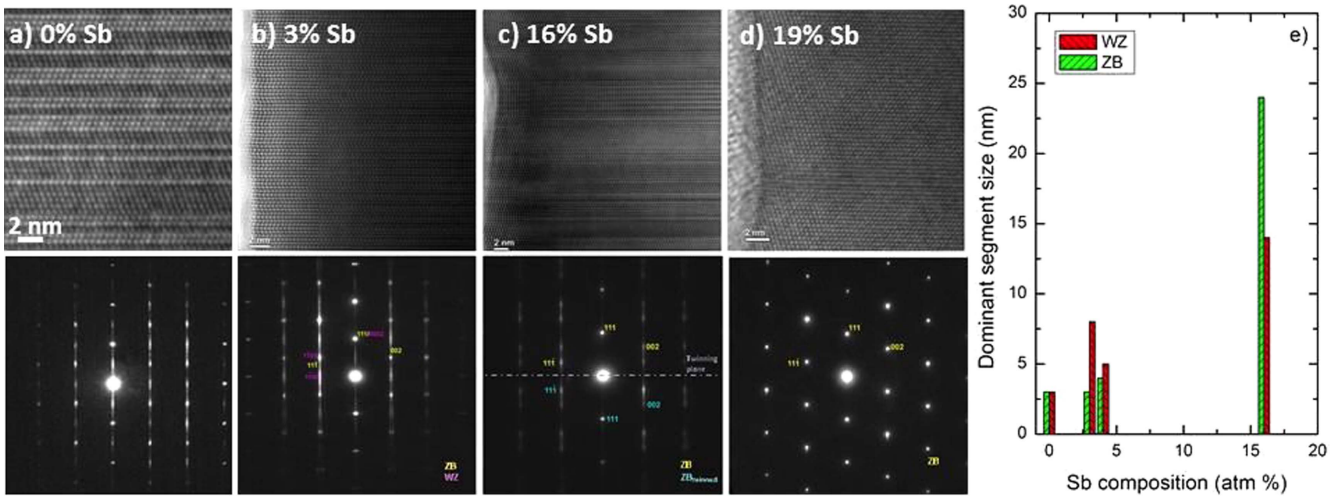

Figure 6. High-resolution TEM images of the InAs NWs (a) and InAsSb NWs with an Sb content of 3% (b), 16% (c), 19% (d), and the average segment size of the ZB and WZ segments in the InAsSb NWs as a function of Sb content (e).

(111)ZB/(0002)WZ planes. It can be seen that the streaks get weaker with more Sb incorporation, and for the NWs with 19% Sb, the diffraction patterns only show spots, which implies the pure phase of the NWs.

The evolution of the crystalline properties was attributed to an enhanced modification of the thermodynamic process in MBE growth induced by both Sb incorporation and the use of droplets in the growth [13, 17]. We previously reported [13] that with an increasing Sb incorporation, the crystal structure of InAsSb NWs evolved from a WZ/ZB mixture to one initially dominated by WZ, then to one dominated by ZB while Sb content was above 4%. Dheeraj *et al* [41] have also reported that the presence of Sb favours ZB phase formation in GaAsSb NWs. It should be noted that this crystal evolution in InAsSb NW growth is further enhanced in droplet-assisted epitaxy due to the additional factor of the modification of the droplet contact angle. Furthermore, these HRTEM images also reveal the presence of various stacking faults in droplet-assisted MBE-grown NWs, such as grain boundaries, rotation twins etc. We have found that the incorporation of Sb is capable of reducing the density of the stacking faults [13], which is in agreement with the observations reported by J Marion *et al* [17]. This is in turn anticipated to improve the optical properties of the resulting NWs. This observation indicates that droplet-assisted growth is a favourable technique for obtaining high-quality NWs. It should be noted that the optical properties could be further improved by suppressing the surface states, which is the major factor impeding the development of NW optoelectronic devices.

In conclusion, we report optically efficient InAsSb NWs with an Sb content of up to 19% covering the entire mid-wavelength infrared, i.e. 3.0–5.1 μm. Although the higher Sb incorporation induces broader Sb fluctuations within single NWs, we found that Sb incorporation effectively improves the optical properties of the InAsSb NWs. The optical properties progress from multi-peak emissions containing a significant amount of defects/impurity-related emission, to single peak emission persisting up to room temperature. This was attributed to the high crystalline quality of the NWs obtained via optimized droplet-assisted epitaxy. Built on this advanced growth technique, we obtained, for the first time, a long wavelength emission of 5.1 μm in InAsSb NWs. This study paves the way to utilizing InAsSb NWs to fabricate highly efficient silicon-based MWIR and FWIR photodetectors which can operate at room temperature.

Acknowledgments

The authors would like to thank the EPSRC Lancaster Impact Acceleration Account and Gas Sensing Solutions for their financial support. SJ and CXR thank the MOST 973 program (2014CB643901) for their support in the ssFTIR-PL experiments.

Notes

The authors declare no competing financial interest.

Author contributions

Q D Z J S and C J J conceived and designed the experiments, led the research and wrote the paper. H A and Z M J contributed to the MBE growth. X R C and X C performed the PL measurements and analyzed the data. A M S performed the TEM measurements and analysis. Y C C and J Y L performed the XRD measurements and analysis. P Y and K D performed the SEM measurements and analyzed the data.

References

[1] Mårtensson T, Patrik C, Svensson T, Wacaser B A, Larsson M W, Seifert W, Deppert K, Gustafsson A, Wallenberg L R and Samuelson L 2004 Epitaxial III−V nanowires on silicon *Nano Lett.* **4** 1987

[2] Battaglia C, Xu J, Zheng M, Yin X, Hettick M, Chen K, Haegel N and Javey A 2014 Enhanced near-bandgap response in InP nanopillar solar cells *Adv. Energy Mater.* 1400061

[3] Xu S, Hansen B J and Wang Z L 2010 Piezoelectric-nanowire-enabled power source for driving wireless microelectronics Q4 *Nature Commun.* (https://doi.org/10.1038/ncomms1098)

[4] Chen S-Y *et al* 2013 Influence of catalyst choices on transport behaviors of InAs NWs for high-performance nanoscale transistors *Phys. Chem. Chem. Phys.* **15** 2654

[5] Saxena D, Mokkapati S, Parkinson P, Jiang N, Gao Q, Tan H H and Jagadish C 2013 Optically pumped room-temperature GaAs nanowire lasers *Nat. Photon.* **7** 963

[6] Olson B V, Shaner E A, Kim J K, Klem J F, Hawkins S D, Murray L M, Prineas J P, Flatte M E and Boggess T F 2012 Time-resolved optical measurements of minority carrier recombination in a mid-wave infrared InAsSb alloy and InAs/InAsSb superlattice *Appl. Phy. Lett.* **101** 092109

[7] Wallart X, Lastennet J, Vignaud D and Mollot F 2005 Performances and limitations of InAs/InAlAsInAs/InAlAs metamorphic heterostructures on InP for high mobility devices *Appl. Phys. Lett.* **87** 043504

[8] Polman A and Atwater H A 2012 Photonic design principles for ultrahigh-efficiency photovoltaics *Nat. Mater.* **11** 174

[9] Law Lori M, Greene E, Johnson J C, Saykally R and Yang P 2005 Nanowire dye-sensitized solar cells *Nat. Mater.* **4** 455

[10] Kelzenberg Shannon M D, Boettcher W, Petykiewicz J A, Turner-Evans D B, Putnam M C, Warren E L, Spurgeon J M, Briggs R M, Lewis N S and Atwater H A 2010 Enhanced absorption and carrier collection in Si wire arrays for photovoltaic applications *Nat. Mater.* **9** 239

[11] Dey A W, Borg B M, Ganjipour B, Ek M, Dick K A, Lind E, Thelander C and Wernersson L-E 2013 High-current GaSb/InAs(Sb) nanowire tunnel field-effect transistors *IEEE Electron. Device Lett.* **34** 211

[12] Nguyen B-M, Taur Y, Picraux S T and Dayeh S A 2014 Diameter-independent hole mobility in Ge/Si core/shell nanowire field effect transistors *Nano Lett.* **14** 585

[13] Zhuang Q D, Anyebe E A, Chen R, Liu H, Sanchez A M, Rajpalke M K, Veal T D, Wang Z M, Huang Y Z and Sun H D 2015 Sb-induced phase control of InAsSb nanowires grown by molecular beam epitaxy *Nano Lett.* **15** 1109

[14] Farrell A C, Lee W-J, Senanayake P, Haddad M A, Prikhodko S V and Huffaker D L 2015 High-quality InAsSb nanowires grown by catalyst-free selective-area metal–organic chemical vapor deposition *Nano Lett.* **15** 6614

[15] Anyebe E A, Rajpalke M K, Veal T D, Jin C J, Wang Z M and Zhuang Q D 2005 Surfactant effect of antimony addition to the morphology of self-catalyzed $InAs_{1-x}Sb_x$ nanowires *Nano Res.* **8** 1309

[16] Anyebe E A *et al* 2015 Realization of vertically aligned, ultrahigh aspect ratio InAsSb nanowires on graphite *Nano Lett.* **15** 4348

[17] Marion J, Sourribes L, Isakov I, Panfilova M, Liu H and Warburton P A 2014 Mobility enhancement by Sb-mediated minimisation of stacking fault density in InAs nanowires grown on silicon *Nano Lett.* **14** 1643

[18] Potts H, Friedl M, Amaduzzi F, Tang K, Tütüncüoglu Ġzde, Matteini F, Lladó E A, McIntyre P C and Fontcuberta i Morral A 2016 From twinning to pure zincblende catalyst-free InAs(Sb) nanowires *Nano Lett.* **16** 637

[19] Du W-N, Yang X-G, Wang X-Y, Pan H-Y, Ji H-M, Luo S, Yang T and Wang Z-G 2014 The self-seeded growth of InAsSb nanowires on silicon by metal-organic vapor phase epitaxy *J. Crystal Grow.* **396** 33

[20] Borg B M, Dick K A, Eymery J and Wernersson L-E 2011 Enhanced Sb incorporation in InAsSb nanowires grown by metalorganic vapor phase epitaxy *Appl. Phys. Lett.* **98** 113104

[21] Johannes Svensson N A, Neimantas Vainorius B M, Borg and Wernersson L-E 2013 Diameter-dependent photocurrent in InAsSb nanowire infrared photodetectors *Nano Lett.* **13** 1380

[22] Ercolani D, Gemmi M, Nasi L, Rossi F, Pea M, Li A, Salviati G, Beltram F and Sorba L 2012 Growth of InAs/InAsSb heterostructured nanowires *Nanotechnol.* **23** 115606

[23] Sun M H, Leong E S P, Chin A H, Ning C Z, Cirlin G E, Samsonenko Y B, Dubrovskii V G, Chuang L and Chang-Hasnain C 2010 Photoluminescence properties of InAs nanowires grown on GaAs and Si substrates *Nanotechnol.* **21** 335705

[24] Koblmuller G, Vizbaras K, Hertenberger S, Bolte S, Rudolph D, Becker J, Doblinger M, Amann M C, Finley J J and Abstreiter G 2012 Diameter dependent optical emission properties of InAs nanowires grown on Si *Appl. Phys. Lett.* **101** 053103

[25] Sun M H, Joyce H J, Gao Q, Tan H H, Jagadish C and Ning C Z 2012 Removal of surface states and recovery of band-edge emission in InAs nanowires through surface passivation *Nano Lett.* **12** 3378

[26] Moller M, de Lima M M Jr, Cantarero A, Chiaramonte T, Cotta M A and Iikawa F 2012 Optical emission of InAs nanowires *Nanotechnol.* **23** 375704

[27] Allen J E *et al* 2008 High-resolution detection of Au catalyst atoms in Si nanowires *Nat. Nanotechnol.* **3** 168

[28] Breuer S, Pfuller C, Flissikowski T, Brandt O, Grahn H T, Geelhaar L and Riechert H 2011 Suitability of Au- and self-assisted GaAs nanowires for optoelectronic applications *Nano Lett.* **11** 1276

[29] Cheze C *et al* 2010 Direct comparison of catalyst-free and catalyst-induced GaN nanowires *Nano Res.* **3** 528–36

[30] Sarney W L and Svensson S P 2015 *J. Vac. Sci. Technol.* B **33** 060604–1

[31] Shao J, Lu W, Lu X, Yue F, Li Z, Guo S and Chu J 2006 *Rev. Sci. Instrum.* **77** 063104

[32] Shao J, Chen L, Lu W, Lu X, Zhu L, Guo S, He L and Chu J 2010 *Appl. Phys. Lett.* **96** 121915

[33] Gladkov P, Nohavica D, Sourek Z, Litvinchuk A P and Iliev M N 2006 Growth and characterization of InAs layers obtained by liquid phase epitaxy from Bi solvents *Semicond. Sci. Technol.* **21** 544

[34] Grober R D, Drew H D, Chyi J I, Kalem S and Morkoc H 1989 Infrared photoluminescence of InAs epilayers grown on GaAs and Si substrates *J. Appl. Phys.* **65** 4079

[35] Zhang L J, Luo J W, Zunger A, Akopian N, Zwiller V and Harmand J C 2010 Wide InP nanowires with wurtzite/zincblende superlattice segments are type-II whereas narrower nanowires become type-I: an atomistic pseudopotential calculation *Nano Lett.* **10** 4055

[36] Murayama M and Nakayama T 1994 Chemical trend of band offsets at wurtzite/zinc-blende heterocrystalline semiconductor interfaces *Phys. Rev.* B **49** 4710

[37] Svensson S P, Sarney W L, Hier H, Lin Y, Wang D, Donetsky D, Shterengas L, Kipshidze G and Belenky G 2012 Band gap of $InAs_{1-x}Sb_x$ with native lattice constant *Phys. Rev.* B **86** 245205

[38] Vurgaftman I, Meyer J R and Ram-Mohan L R 2001 Band parameters for III–V compound semiconductors and their alloys *J. Appl. Phys.* **89** 5815

[39] Yen M Y, People R, Wecht K W and Cho A Y 1988 Long-wavelength photoluminescence of $InAs_{1-x}Sb_x$ ($0 < x < 1$) grown by molecular beam epitaxy on (100) InAs *Appl. Phys. Lett.* **52** 489

[40] Fang Z M, Ma K Y, Jaw D H, Cohen R M and Stringfellow G B 1990 Photoluminescence of InSb, InAs, and InAsSb grown by organometallic vapor phase epitaxy *J. Appl. Phys.* **67** 7034

[41] Dheeraj D L, Patriarche G, Zhou H, Hoang T B, Moses A F, Grønsberg S, van Helvoort Antonius T J, Fimland B-O and Weman H 2009 Growth and characterization of wurtzite

GaAs nanowires with defect-free Zinc blende GaAsSb inserts *Nano Lett.* **8** 4459